Power exchanged between subsystems with non-diffuse fields in statistical energy analysis

V. Tyrode, N. Totaro, Laurent Maxit, A. Le Bot

Power exchanged between subsystems with non-diffuse fields in statistical energy analysis.

V. Tyrode,[1] N. Totaro,[2] L. Maxit,[2] and A. Le Bot[1, a]

[1] *Univ Lyon, Ecole Centrale de Lyon, Laboratory of tribology and system dynamics, UMR CNRS 5513, 69134, Ecully, France*

[2] *Univ Lyon, INSA Lyon, LVA, EA677, 69621 Villeurbanne, France*

(Dated: 25 April 2023)

This article is a discussion on the necessity of the assumption of diffuse field in statistical energy analysis (SEA) and the validity of the coupling power proportionality which states that the vibrational power exchanged between coupled subsystems is proportional to the difference of their modal energies. It is proposed to re-formulate the coupling power proportionality in terms of *local energy density* instead of *modal energy*. We show that this generalized form remains valid even if the vibrational field is not diffuse. Three causes of lack of diffuseness have been studied: coherence of rays in symmetrical geometries, non ergodic geometries, and the effect of high damping. Numerical simulations and experimental results conducted on flat plates in flexural vibration are provided to support these statements.

[a] alain.le-bot@ec-lyon.fr

I. INTRODUCTION

Predicting the dynamical behaviour of structures in the low frequency range is a problem that is largely overcome today. But at high frequencies, the classical methods like the well-known finite element analysis become quickly inefficient. This has motivated the emergence of methods with a lower numerical cost like statistical energy analysis (SEA)[1–4] (see Ref.[5] for an up-to-date synthesis of the theory).

The principle of SEA is to subdivide a complex system into subsystems and to analyze their exchanges of vibrational energy. The main result which allows a systemic approach is the so-called *coupling power proportionality* which claims that the power exchanged between two lightly coupled subsystems is proportional to the difference of their modal energies also referred to as vibrational temperatures. It is in this way that SEA may be interpreted as the theory of thermodynamics of sound and vibration[6].

The foundation of the coupling power proportionality must be found in the assumption of modal energy equipartition, or equivalently, in the assumption of diffuse field (see Refs.[7,8] for a definition of diffuse field). Several alternative theories have been proposed to relax these assumptions. The theory of statistical energy modal distribution analysis (SmEdA)[9,10] extends SEA to mid-frequencies by setting power balance equations to individual modes instead of mode packets making it possible not to assume energy equipartition. Whereas non-diffuse fields are naturally accounted for in the framework of geometrical acoustics for instance by the approach of radiative energy transfer equations[11–14] and more recently by dynamical energy analysis[15–17], these two approaches have the advantage to establish clearly

the link between geometrical acoustics and SEA[18] and even to propose a continuum between a full ray-tracing analysis and a more gross SEA analysis[16].

In the wave approach of SEA[19,20], the coupling power proportionality is naturally derived from the analysis in terms of plane waves impinging on the boundary separating the two subsystems[21,22]. The advantage of this approach is that it provides explicit formulas for the coupling loss factors that are also applicable to the case of non isotropic incidence. But this type of analysis is restricted to the hypothesis of rays and its main innuendo the principle of locality. In case of point connected subsystems, the applicability of locality is questionable although the coupling power proportionality remains valid.

There is however an interest to test the validity of the coupling power proportionality beyond the assumption of diffuse field in the most general case. Some particular effects may frustrate a uniform and isotropic distribution of energy and therefore may constitute an obstacle to application of SEA. For instance, symmetries in geometry can lead to a non-homogeneity of the field. In a circular plate, one observe the presence of a caustic passing through the point of excitation where the energy density has a higher level[23]. Vibrational energy is also enhanced on points and lines outside source position for spatial symmetry reasons[24]. This phenomenon is caused by an effect of coherence in ray propagation. This energy enhancement has been observed for instance by deflectometry[25] and with vibrational field measurements with a laser vibrometer[26].

In this context, the objective of this study is to check if the coupling power proportionality is still valid for point connected subsystems in situations where the field is not fully homogeneous.

The paper is organized as follows. Section II reminds of theoretical aspects of SEA and proposes a local formulation of the coupling power proportionality. Section III presents four examples of vibrational fields for which the energy is not perfectly uniformly distributed. The validity of the local form of the coupling power proportionality is tested by numerical simulations in Section IV and by experiments in Section V. Finally, in Section VI, the notion of vibrational temperature is introduced and a thermodynamic interpretation of these results is proposed.

II. BASICS OF SEA

The principle of statistical energy analysis is to divide a complex system into simple subsystems and, for each subsystem, to estimate the power supplied by external sources, the losses of vibrational energy by natural processes of dissipation, and the exchange of energy with other subsystems.

A. SEA assumptions

The theory of statistical energy analysis requires three assumptions.

- (H1) The sources are random, stationary, wide band, and uncorrelated;
- (H2) The couplings between subsystems are conservative and weak;
- (H3) The vibrational field is diffuse in all subsystems.

These assumptions have been discussed in the literature (see Ref.[27] for a review of them) and some of them have been partly relaxed. The consequence of strong coupling is discussed

in Ref.[28,29]. The necessity of conservative coupling is justified in Ref.[30]. Since the purpose of this article is only to investigate the influence of diffuse field in the subsystems on SEA results, the rest of the discussion will be held under the condition that (H1) and (H2) apply.

The diffuse field assumption is certainly the most difficult to satisfy in practice. A diffuse field is defined as a homogeneous and isotropic superposition of plane waves whose phase is random.

A solution to obtain a diffuse field is to excite the structure with a uniform distribution of point forces which are δ-correlated in space and time (rain-on-the-roof). In that case, all modes receive an equal amount of energy and if their damping ratio is the same, they store a same amount of energy.

With a single point force, the state of diffuse field is reached when the source is random and the structure sufficiently reverberant. Then, a large number of modes weakly damped contribute to the vibrational energy within the system. The number of resonant modes must be large to avoid a modal effect by a dominating mode and the damping must be low to ensure the mixing of energy by rays that propagate over a long range and are reflected throughout the subsystem.

To check if the vibrational field is diffuse in the subsystems validity diagrams have been proposed[31]. This diagram plots a criterion of uniformity of energy in the frequency, damping loss factor plane. The zone of diffuse field is confined by two lines marking the conditions of large number of resonant modes and weak attenuation of rays during a mean-free-path. Based on the location of each subsystem in these diagrams, it is possible to anticipate the applicability of SEA[32].

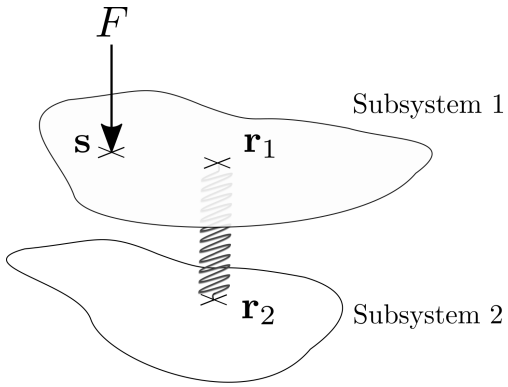

FIG. 1. Two flat subsystems coupled with a spring at point $\mathbf{r}_1$ on plate 1 and point $\mathbf{r}_2$ on plate 2. Plate 1 is excited with a wide-band stationary random force F at point $\mathbf{s}$.

B. The law of coupling power proportionality

Let us consider two flat plates in flexural vibration weakly coupled by a spring attached at point $\mathbf{r}_1$ on plate 1 and point $\mathbf{r}_2$ on plate 2 as shown in Figure 1. Subsystem 1 is excited by a wide band random force $F(t)$ at point $\mathbf{s}$. We assume that the field is diffuse in both plates.

Under these conditions, the coupling power proportionality states that the expectation of the power P (W) exchanged between connected subsystems is

$$P = \beta \left(\frac{E_1}{n_1} - \frac{E_2}{n_2} \right). \tag{1}$$

where E_i is the expectation of vibrational energy (J) in subsystem i, n_i the modal density (modes per rad/s), and β a dimensionless coefficient. In particular, this law shows that the vibrational energy always flows from subsystems having a large modal energy to that with a lower modal energy.

In the case of flat plates in flexural vibration, the modal density is given by

$$n_i = \frac{A_i}{4\pi}\sqrt{\frac{m_i}{D_i}} \tag{2}$$

where A_i is the area (m^2) , m_i is the mass per unit area (kg/m^2), and $D_i = E_i h_i^3/12(1-\nu_i^2)$ the bending stiffness (N.m) with E_i the Young modulus (Pa), h_i the thickness (m) and ν_i the Poisson coefficient of plate i. Note that the modal density of a plate does not depend on the frequency and is proportional to its area.

When the plates are coupled by a spring of stiffness K, the coupling coefficient is

$$\beta = \frac{K^2}{32\pi\omega_c^2\sqrt{m_1 m_2 D_1 D_2}} \tag{3}$$

where ω_c is the central frequency (rad/s) of the wide-band random source.

C. Generalized coupling power proportionality

Introducing the mean energy density e_i (J/m^2) defined as $e_i = E_i/A_i$ the energy per unit area into Eq. (1) gives

$$P = \beta\left(\frac{e_1 A_1}{n_1} - \frac{e_2 A_2}{n_2}\right). \tag{4}$$

This form suggests a generalization to the case where the energy is not uniformly distributed into the subsystems. Substituting the local energy density $e_i(\mathbf{r})$ at the coupling point $\mathbf{r}$ to the mean energy density e_i in Eq. (4) leads to

$$P = \beta\left(\frac{e_1(\mathbf{r}_1) A_1}{n_1} - \frac{e_2(\mathbf{r}_2) A_2}{n_2}\right). \tag{5}$$

where $e_1(\mathbf{r}_1)$ and $e_2(\mathbf{r}_2)$ are respectively the energy densities at point $\mathbf{r}_1$ on subsystem 1 and point $\mathbf{r}_2$ on subsystem 2.

In Eq. (1) appear the modal energies E_i/n_i. Since most of modes expand over the whole subsystem, these are global quantities. But Eq. (5) is written in terms of energy densities $e_i(\mathbf{r})$ which are local quantities. Furthermore, the ratio $A_i/n_i = 4\pi\sqrt{D_i/m_i}$ is also a local since it only depends on local characteristics of the plate (m_i and D_i).

When the vibratory fields are diffuse, Eqs. (1) and (5) are equivalent. However, it is relevant to wonder if the latter remains valid in cases where the local energy density $e_i(\mathbf{r})$ is not equal to the mean energy density e_i. The rest of the paper focuses on this question.

III. DIFFUSE AND NON-DIFFUSE FIELD

Three geometries of plates are considered: a Bunimovich stadium plate, a rectangular plate, and a circular plate (see Fig. 2). These shapes have been chosen because they are representative of various behaviours in ray propagation[33]. A Bunimovich stadium is a chaotic billiard[34]. Almost all rays propagating and specularly reflecting on boundaries explore the entire phase space (all positions and all directions) with an equal probability of presence. The vibrational field resulting from a large number of rays emitted by a single source is therefore naturally diffuse.

A rectangular billiard is an integrable dynamical system. A ray does not generally explore the entire phase space. It generally passes near all points of the rectangle excepted if its path is closed. But the angle of incidence is always the same on small edges and the same (with possibly a different value) on large edges (with positive or negative sign). Thus the ray can take only four directions during its propagation. The resulting field is therefore

141 homogeneous but not isotropic. However, if a point source emits many rays equally in all
142 directions, then it enforces the field to be isotropic and therefore to be diffuse.

143 A circular billiard is also an integrable dynamical system. The angle of incidence of a
144 ray on the boundary is constant during its propagation. The ray forms a circular caustic
145 that never get into. Thus the ray explores entirely the part of the disk located outside this
146 circular caustic excepted if its path is closed. But the ray does not explore the part of the
147 disk located inside the circular caustic. The phase space is not entirely explored and the
148 resulting vibrational field is never diffuse neither with a single ray nor with an isotropic
149 source emitting rays in all directions.

150 A. Direct numerical simulation of energy field

151 In all subsequent numerical simulations, the values of the mechanical parameters are the
152 followings. The Young modulus is $E = 203$ GPa, the mass density $\rho = 8010$ kg.m^{-3} and
153 Poisson's ratio $\nu = 0.3$. The thickness of the three plates is $h = 2$ mm. Their dimensions
154 are represented in Figure 2. They all have an area about $A = 0.25$ m^2. Two values of
155 the damping loss factor are used: $\eta = 0.002$ in case of light damping and $\eta = 0.2$ when
156 the damping is strong. A unique external force $F(t)$ is applied to plate 1 at point $\mathbf{s}$. The
157 excitation point is located at x=176 mm, y=164 mm in the stadium plate, at x=120 mm,
158 y=70 mm in the rectangular plate, and at x=150 mm, y=150 mm in the circular plate. The
159 force is a stationary random process of power spectral density S_0 constant in the octave
160 band $\Delta\omega$ centred on $\omega_c = 2\pi \times 4000$ rad.s^{-1} and zero elsewhere.

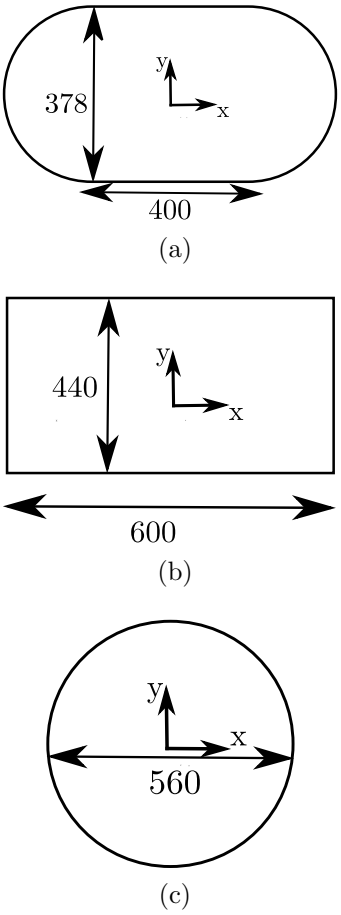

FIG. 2. Shape and dimensions of plates in mm. (a); Bunimovich stadium, (b); Rectangular plate, and (c); Circular plate.

With these values, we may estimate the mean-free-path $\bar{l} = \pi A/P$ where A is the plate area and P the perimeter. For the stadium plate $\bar{l} = 0.42$ m, for the rectangular plate $\bar{l} = 0.40$ m, and for the circular plate $\bar{l} = 0.44$ m. The group velocity is $c_{\rm g} = 553$ m/s and the wavelength is $\lambda = 7$ cm at 4 kHz which is six times lower than the mean-free-path. This justifies that a geometrical acoustics approximation applies. The modal density is about 0.0065 mode per rad/s and therefore the number of resonant modes in the octave band 4 kHz is about $N = 120$ which is high enough to consider a statistical population of modes.

Finally, the attenuation per mean-free-path is $\bar{m} = \eta\omega\bar{l}/c_g$ is $\bar{m} = 0.04$ when the damping is light ($\eta = 0.002$). This means that $1 - \exp(-\bar{m}) = 4$ % of the energy is lost between two successive reflections of a ray. This low value ensures that rays experience a large number of reflections before to vanish. But this value grows up to 98 % when the damping is high ($\eta = 0.2$) meaning that rays loss almost all their energy before the first reflection.

The expectation of vibrational energy density $e(\mathbf{r})$ at position $\mathbf{r}$ is $e(\mathbf{r}) = m < \dot{u}^2 >$ where $\dot{u}$ is the vibrational velocity and $< . >$ denotes the random expectation operator. The variance of $\dot{u}$ is $\int S_{\dot{u}\dot{u}}\,\mathrm{d}\omega/2\pi$ where $S_{\dot{u}\dot{u}}$ is the power spectral density of $\dot{u}$. In addition, $S_{\dot{u}\dot{u}} = S_0\omega^2|H|^2$ where $H(\mathbf{r}, \mathbf{s}; \omega)$ is the receptance (frequency response function between the force F at point $\mathbf{s}$ and deflection u at point $\mathbf{r}$). Since the power spectral density S_0 of the force is constant within $\Delta\omega$, this gives

$$e(\mathbf{r}) = \frac{mS_0}{\pi}\int_{\Delta\omega}\omega^2|H(\mathbf{r};\mathbf{s};\omega)|^2\,\mathrm{d}\omega. \tag{6}$$

In the numerical estimation of this integral, the angular frequency step is chosen as $\omega\eta/4\sqrt{2}$. The receptance $H(\mathbf{r}, \mathbf{s}; \omega)$ in terms of natural frequencies ω_n and mode shapes Ψ_n is obtained with a modal expansion

$$H(\mathbf{r};\mathbf{s};\omega) = \sum_{n>0}\frac{\Psi_n(\mathbf{s})\Psi_n(\mathbf{r})}{m(\omega_n^2 - \omega^2 + \mathrm{i}\eta\omega_n\omega)}. \tag{7}$$

where i is the imaginary unit. The modes are calculated by the finite element method with MSC/NASTRAN 2021.1 up to the frequency 6 kHz to ensure that $H(\mathbf{r};\mathbf{s};\omega)$ is correctly estimated within the entire octave band 4 kHz. About 240 modes have been found.

The inverse participation ratio is defined as the fourth-order moment of vibrational velocity $\dot{u}$ or equivalently as the second-order moment of energy density $e(\mathbf{r})$

$$I_p = \frac{\frac{1}{A}\int e^2(\mathbf{r})\,\mathrm{d}\mathbf{r}}{(\frac{1}{A}\int e(\mathbf{r})\,\mathrm{d}\mathbf{r})^2}. \tag{8}$$

Its definition imposes $I_p \geq 1$. When the vibrational energy is uniformly distributed over the subsystem ($e(\mathbf{r}) = \text{cste}$), I_p goes to one. But when the vibrational energy distribution is not uniform and presents large fluctuations from one point to another one, I_p can take arbitrarily high values. We shall adopt the criterion $I_p \leq 2$ to characterize a uniform distribution of energy.

B. Diffuse field

Fig. 3(a) shows the distribution of energy density in a lightly damped stadium-shaped plate with clamped edges excited by a random force at point S_1. Fig. 3(b) shows the distribution of energy density in a lightly damped rectangular plate with simply supported edges excited by a random force.

The values of I_p for stadium and rectangular plates are given in Table I. They are both lower than 2 (respectively 1.09 for the stadium and 1.38 for the rectangle) so that following this criterion, the vibrational field is uniformly distributed over the rectangular plate and the stadium.

But even if the inverse participation ratio is low, the vibrational field is not fully spatially homogeneous. The energy distribution exhibits patterns with energy enhancement. For the stadium shape, four points with energy enhancement are visible. They are noted $\mathbf{s}_1$, $\mathbf{s}_2$, $\mathbf{s}_3$,

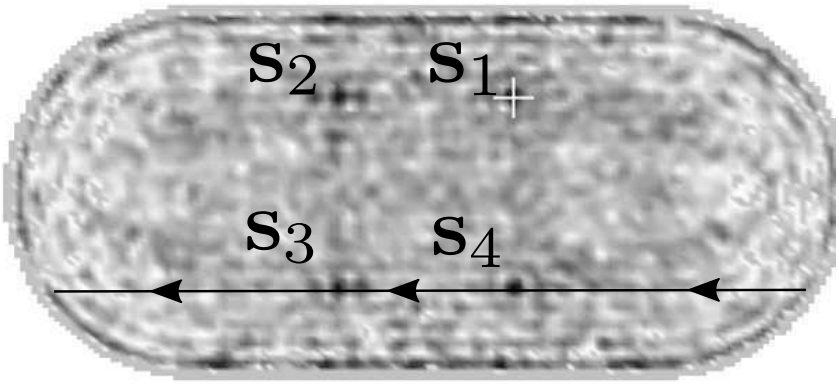

(a)

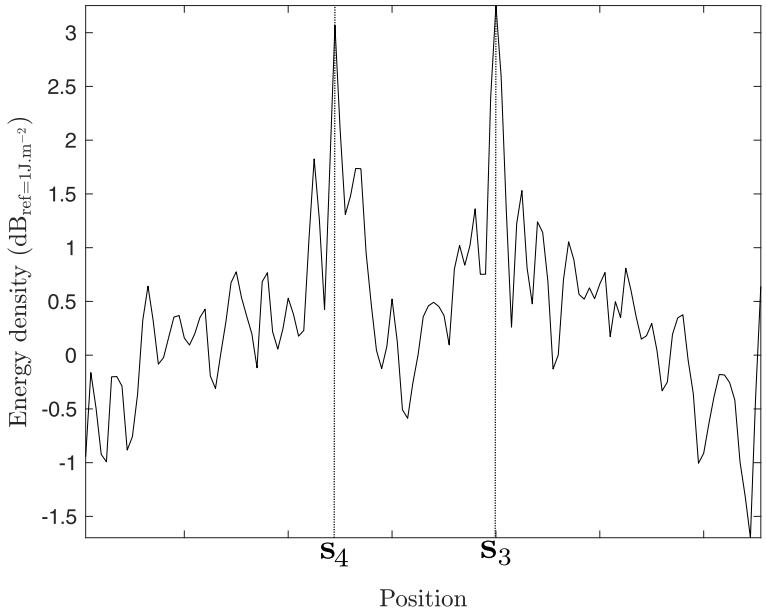

(b)

FIG. 3. (a) Numerical simulation of vibrational energy distribution (dB) in a stadium thin plate lightly damped ($\eta = 2 \times 10^{-3}$) with clamped edges and excited by a wide-band random force. The cross indicates the force position. (b) Vibrational energy in dB along the black line.

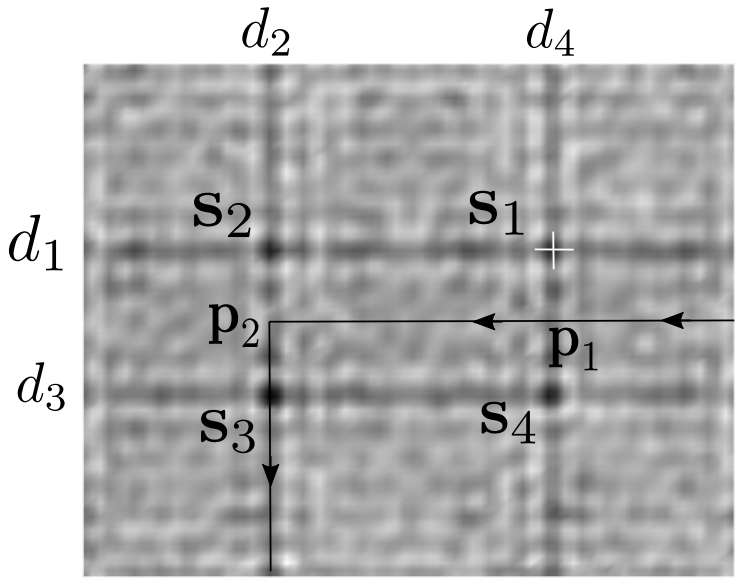

(a)

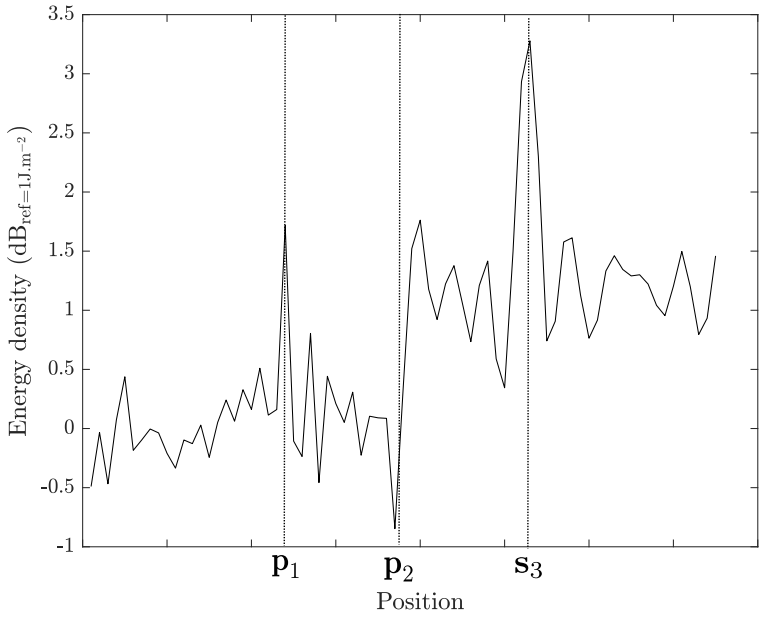

(b)

FIG. 4. (a) Numerical simulation of vibrational energy distribution (dB) in a rectangular thin plate lightly damped ($\eta = 2 \times 10^{-3}$) with simply supported edges and excited by a wide-band random force. The cross indicates the force position. (b) Vibrational energy in dB along the black line.

TABLE I. Inverse participation ratio for the four plates excited by a random force in the octave centred on 4 kHz.

	Stadium $\eta = 2 \times 10^{-3}$	Rectangle $\eta = 2 \times 10^{-3}$	Circle $\eta = 2 \times 10^{-3}$	Rectangle $\eta = 0.2$
IPR	1.09	1.38	8.89	4.61

and $\mathbf{s}_4$ in Fig. 3(a). The enhancement factor on these four points is equal to 2 (this effect at the source point is known as coherent backscattering effect[34]). In Fig. 3(b), we can see lines noted d_1, d_2, d_3, and d_4 which form a tic-tac-toe pattern with the driving point at one of the four intersections. In Fig. 4(a), we see a step of about 1.5 dB on points $\mathbf{p}_1$ and $\mathbf{p}_2$. In linear scale, the enhancement factor of energy on these four lines is equal to 3/2. On the four points noted $\mathbf{s}_1$, $\mathbf{s}_2$, $\mathbf{s}_3$, and $\mathbf{s}_4$ located at the intersections of the four lines, the enhancement factor is equal to 9/4 (3.4 dB on point $\mathbf{s}_3$ in Fig. 4(a)).

Several works have shown that a symmetrical mechanical structure excited by a wideband random point force exhibits a pattern of points or lines where the vibrational response is enhanced (see for instance Ref.[26] where a proof of these enhancement factor based on the image source method is provided). These enhancements may be explained in geometrical acoustics by considering the phase of pairs or quadruplets of rays arriving at the receiver points with same phase. They interfere constructively and therefore contribute to the local energy density more than the simple sum of their energies.

C. Non diffuse field

Fig. 5(a) shows the distribution of energy density in a lightly damped circular plate with clamped edges excited by a random force at point S_1. The damping loss factor is low $\eta = 2 \times 10^{-3}$.

From Fig. 5(a) we see that the vibrational energy fluctuates a lot and reaches a maximum on the circle C_1 passing through the excitation point. Furthermore, the diameter passing through the source also shows a higher level of energy. The inverse participation ratio is high (8.89).

The evolution of energy density along a diameter can can be explained again with geometrical acoustics. Each ray starting from the source turns into the circle by conserving its angle of reflection. Excepted for periodic orbits, the ray forms a circular caustic that is never crossed by it. The ray does not explore the entire disk and the resulting distribution of energy is henceforth not uniform. The combination of large number rays emitted in all directions from the source point gives roughly the distribution of energy observed in Fig. 5(b). It is not necessary to invoke interference of rays to explain this distribution.

The enhancement of energy on the diameter passing through the source point stems from another phenomenon. This is again a phenomenon of constructive interference. The spatial symmetry of the circle imposes that each ray starting from the source and arriving at any point of this diameter, admits a symmetrical ray starting from the source and arriving at the same point. Both direct and symmetrical rays have same length and therefore have the same phase at arrival. They interfere constructively giving the observed enhancement.

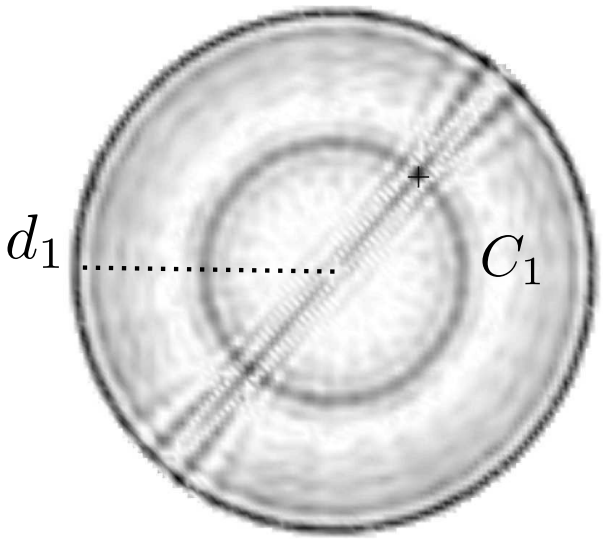

(a)

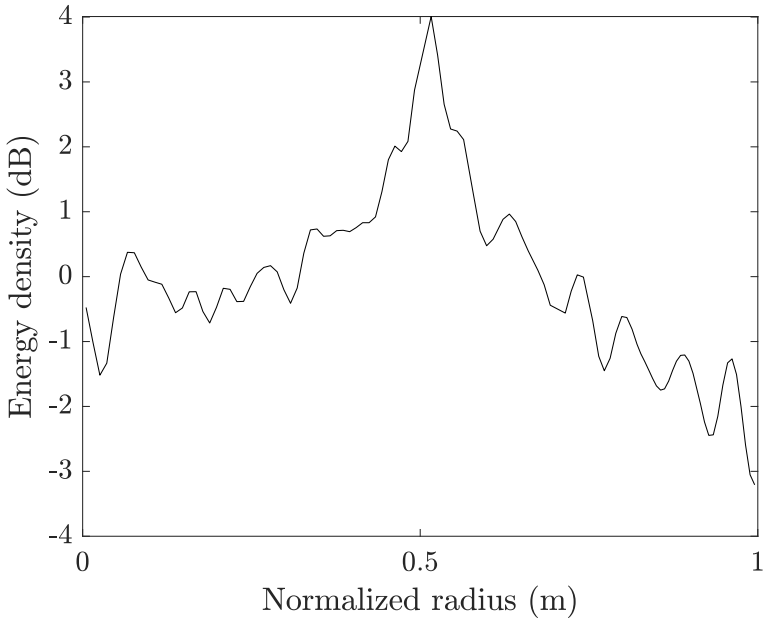

(b)

FIG. 5. (a) Numerical simulation of vibrational energy distribution (dB) in a circular thin plate lightly damped ($\eta = 2 \times 10^{-3}$) with clamped edges and excited by a wide-band random force. The cross indicates the force position. (b) Vibrational energy in dB along the radius d_1.

A last cause of breaking homogeneity is the influence of strong dissipation. Fig. 6(a) shows the distribution of energy density in a highly damped ($\eta = 0.2$) rectangular plate with simply supported edges excited by a random force at point S_1. Fig. 6(a)a shows the maps of energy density and Fig. 6(b) shows the vibrational energy along the line d_2 while the dashed line is obtained with a reference calculation.

We observe that the distribution of energy is clearly not uniform which is confirmed by the high value (4.61) of the inverse participation. The maximum of energy is reached at the source point from which the energy strongly decreases in a axi-symmetrical way.

We know that the attenuation per mean-free-path is high ($\bar{m} = 3.6$) and that rays loss 98 % of their energy before the first reflection. The vibrational field is therefore dominated by the direct field and the reflected field remains negligible. For the direct field, the energy at distance R from the source is $\exp(-mR)/2\pi c_g R$. The exponential term is the dissipation while the second term is due to the geometric scattering. In Fig. 6(b), we observe that the dashed line (direct field) and the solid line (actual field including reverberation) well fit which confirms the domination of the direct field in the actual field.

IV. NUMERICAL SIMULATION OF EXCHANGED POWER

Let us now turn to the verification of the generalized coupling power proportionality (5) by a numerical approach.

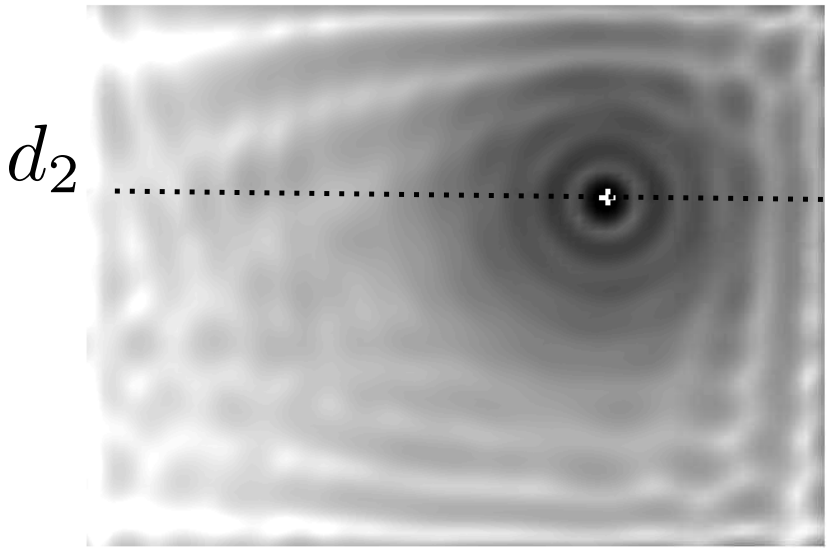

(a)

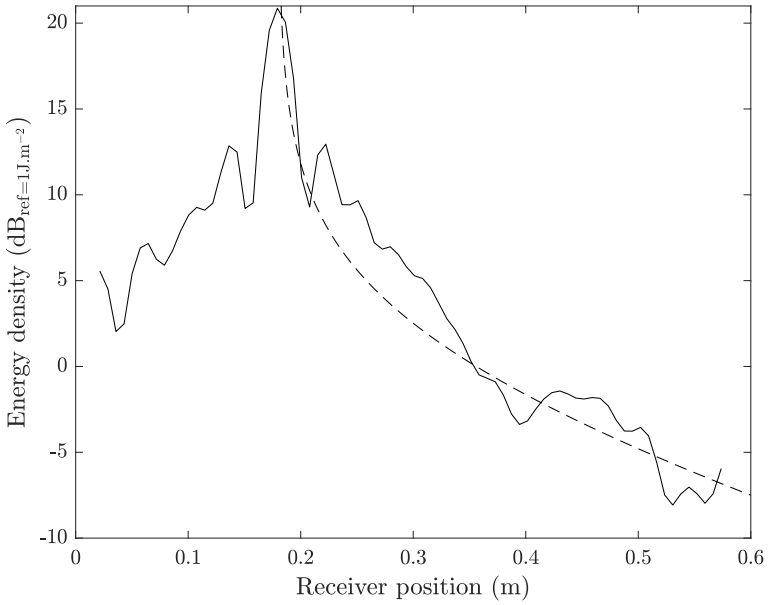

(b)

FIG. 6. (a) Numerical simulation of vibrational energy distribution (dB) in a rectangular thin plate highly damped ($\eta = 0.2$) with simply supported edges and excited by a wide-band random force. The cross indicates the force position. (b) Vibrational energy in dB along the radius d_2.

A. Principle of the simulation

We consider again the three geometries of plates introduced in Section III: the stadium, the rectangle, and the disk. But now, the plates are mechanically coupled by a spring of stiffness K. Each numerical test case consists in two similar plates among the three geometries coupled by the spring whose position may vary to explore zones with different levels of vibrational energy. The spring is attached at point $\mathbf{r}_1$ on plate 1 and at $\mathbf{r}_2$ centre of plate 2. Plate 1 is excited at point $\mathbf{s}$ always with a random force of power spectral density S_0 constant in the octave band $\Delta\omega$. The positions of the point force are the same as in Section III. The exact positions $\mathbf{r}_1$ of the spring will be specified in each numerical simulation.

The expectation of vibrational energy density $e_i(\mathbf{r})$ in plates 1 and 2 is calculated again by Eq. (6). The only difference is concerned with the receptance H which is now the receptance of the *coupled* system. Thus, $H(\mathbf{r}, \mathbf{s}; \omega)$ denotes the deflection at point $\mathbf{r}$ (in plate 1 or 2) of the coupled system excited at point $\mathbf{s}$ (in plate 1).

The expectation of exchanged power via the spring is $P = K < (u_2 - u_1)\dot{u}_1 >= K < u_2\dot{u}_1 >= -K < \dot{u}_2 u_1 >$ where u_i is the deflection of plate i at the coupling point. In terms of receptance, this power becomes

$$P = \frac{KS_0}{\pi} \int_{\Delta\omega} \mathrm{Re}[\mathrm{i}\omega \overline{H}(\mathbf{r}_1, \mathbf{s}; \omega) H(\mathbf{r}_2, \mathbf{s}; \omega)] \, \mathrm{d}\omega \tag{9}$$

where Re denotes the real part, the overbar the complex conjugate, and i the imaginary unit.

The numerical simulation is conducted with the same modes of isolated plates calculated by MSC/NASTRAN in Section II. But instead of using Eq. (7) to calculate H, the receptance

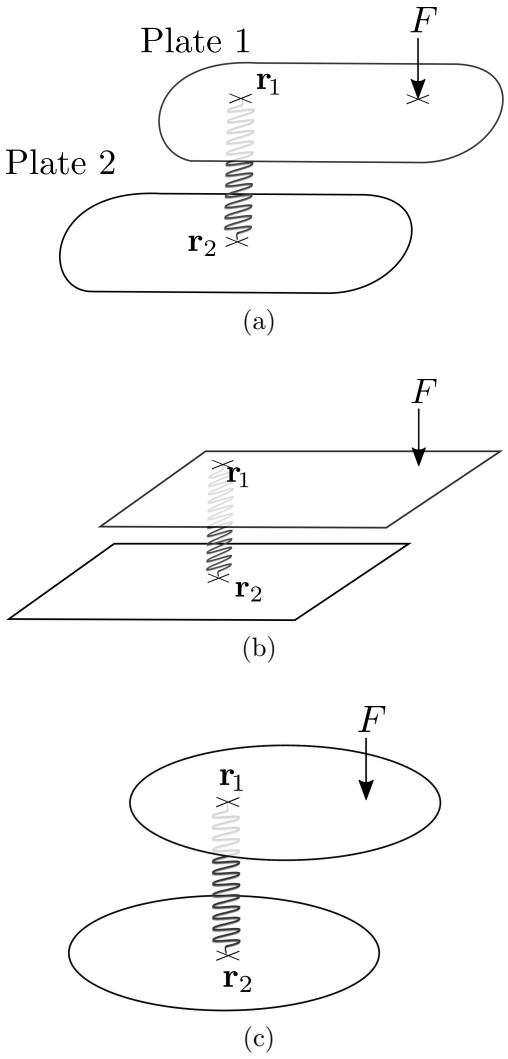

FIG. 7. (a) The stadium-shaped plates, (b) the rectangular plates, and (c) the disk plates coupled with a spring.

of coupled system is derived from the receptances of uncoupled subsystems by introducing the deflections u_1, u_2 at both ends of the spring as unknown and solving a set of two linear equations to determine them (the exact procedure is detailed in Appendix A).

Once, we have computed the energies $e_1(\mathbf{r}_1)$, $e_2(\mathbf{r}_2)$ and the exchanged power P by the above procedure, the coupling coefficient β is estimated by

$$\beta = \frac{P}{\frac{e_1(\mathbf{r}_1)A_1}{n_1} - \frac{e_2(\mathbf{r}_2)A_2}{n_2}}. \tag{10}$$

In particular, we shall compare the numerical determination of β by Eq. (10) with its theoretical value given in Eq. (3).

B. Test cases

All numerical simulations of this Section are conducted on plates whose geometrical and mechanical parameters are those of Section III. In particular, the frequency of excitation is $\omega_c = 2\pi \times 4000$ rad/s and the wavelength is 7 cm to be compared with a mean-free-path of 42 cm. The number of resonant modes is about 120 per subsystem that is 240 for the whole system. The spring stiffness is $K = 1.10^5$ N/m. To ensure that the weak coupling assumption is satisfied, the coupling loss factor defined as $\eta_{12} = \beta/\omega_c n_1$ has to be lower than the damping loss factor η[28]. The coupling loss factors $\eta_{12} = \eta_{21}$ are equal to 3.10^{-6} which is lower than the damping loss factor (2.10^{-3}) and so the coupling is weak enough.

Four simulations are carried out with the four types of diffuse and non-diffuse fields presented in Section III.

1. Stadium plate

The numerical simulation with two coupled stadium plates is presented in Fig. 8(a). In the inset of Fig. 8(a) the stadium is represented and the four points with an energy enhancement of 2 are noted $\mathbf{s}_1$ (the source), $\mathbf{s}_2$, $\mathbf{s}_3$, and $\mathbf{s}_4$. Four other points noted 1

to 4 are chosen at random inside the zone where the field is diffuse. Fig. 8(a) shows a comparison between the exchanged power P determined by Eq. (9) and the difference of local energies $e_1(\mathbf{r}_1)A_1/n_1 - e_2(\mathbf{r}_2)A_2/n_2$ where e_i is determined by Eq. (6). The bold line with the crosses represents the power exchanged between the two plates. The thin line with the stars represents the difference of the local energies. Fig. 8(b) presents the relative error between β determined by Eq. (3) and by Eq. (10).

First, the spring is successively attached at the four points 1 to 4 where the vibrational field is diffuse. It can be seen in Fig. 8(b) that the ratio of P and $e_1(\mathbf{r}_1)A_1/n_1 - e_2(\mathbf{r}_2)A_2/n_2$ (or difference in log-scale) is almost the same for the four points. Furthermore we see in Fig. 8(b) that this ratio is close to the theoretical value of β given in Eq. (3).

Secondly, the spring is successively attached at the four points $\mathbf{s}_1$, $\mathbf{s}_2$, $\mathbf{s}_3$, and $\mathbf{s}_4$. The exchanged power is increased by a step of $10\log(2)$ which corresponds exactly to the enhancement factor of 2. Again, the ratio of P and $e_1(\mathbf{r}_1)A_1/n_1 - e_2(\mathbf{r}_2)A_2/n_2$ is close to the theoretical β.

In all cases, the numerical coupling coefficient is found to be in fine agreement with the theoretical value. The mean relative error between the numerical and theoretical values is 28.8 %.

2. Rectangular plate with light damping

The numerical simulation with two coupled rectangular plates is presented in Fig. 9(a). In the inset of Fig. 9(a) the rectangular plate is represented with the four lines presenting an energy enhancement of 3/2. The five points ($\mathbf{d}_1$, $\mathbf{d}_2$, $\mathbf{d}_3$, $\mathbf{d}_4$ and $\mathbf{d}_5$) are chosen randomly

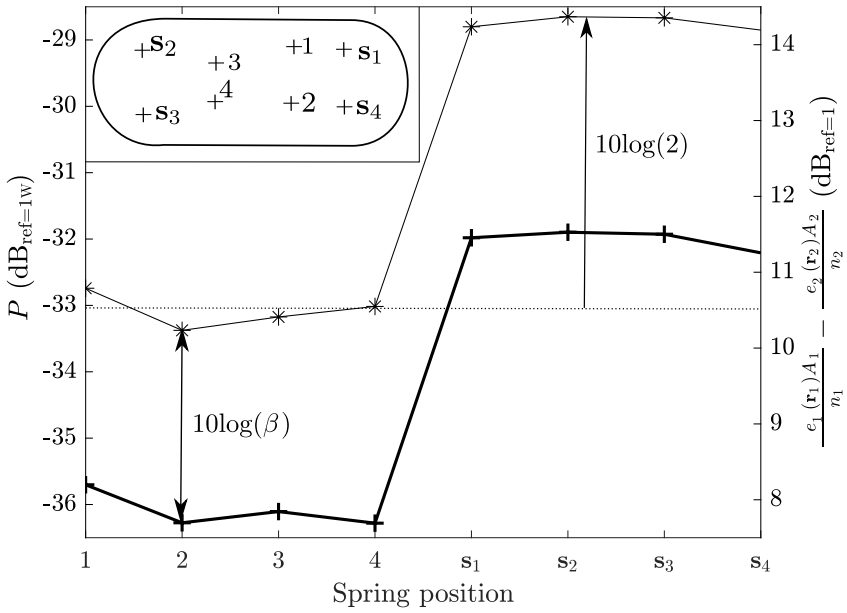

FIG. 8. (a) Comparison between the exchanged power and the difference of local energies. The bold line with the crosses represents the power exchanged between the two plates. The thin line with the stars represents the difference of the local energies. In the insert: stadium plates excited with a random white noise at point $\mathbf{s}_1$. Points with an energy enhancement equal to 2 are noted $\mathbf{s}_1$, $\mathbf{s}_2$, $\mathbf{s}_3$, and $\mathbf{s}_4$. The spring is successively attached to the points noted $\mathbf{s}_1$, $\mathbf{s}_2$, $\mathbf{s}_3$, $\mathbf{s}_4$, 1, 2, 3 and 4. (b) Relative error between the coupling coefficient predicted theoretically with Eq. (3) and numerically with Eq. (10) for two coupled stadium plates excited by a point force on plate 1.

on these four lines. The four points of energy enhancement 9/4 ($\mathbf{s}_1$, $\mathbf{s}_2$, $\mathbf{s}_3$, and $\mathbf{s}_4$) are represented with a cross. Five points noted 1 to 5 are chosen at random inside the zone where the field is diffuse. Fig. 9(a) shows a comparison between the exchanged power P determined by Eq. (9) and the difference of local energies $e_1(\mathbf{r}_1)A_1/n_1 - e_2(\mathbf{r}_2)A_2/n_2$ where e_i is determined by Eq. (6). Fig. 9(b) presents the relative error between β determined by Eq. (3) and by Eq. (10).

First, the spring is successively attached at the five points 1 to 5 where the vibrational field is diffuse. It can be seen in Fig. 9(a) that the ratio of P and $e_1(\mathbf{r}_1)A_1/n_1 - e_2(\mathbf{r}_2)A_2/n_2$ is almost the same for the five points. Furthermore we see in Fig. 9(b) that this ratio is close to the theoretical value of β given in Eq. (3).

Secondly, the spring is successively attached on a point located on a line ($\mathbf{d}_1$, $\mathbf{d}_2$, $\mathbf{d}_3$, and $\mathbf{d}_4$). The exchanged power is increased by a step of $10\log(3/2)$ which corresponds to the enhancement factor of 3/2. Once again, the ratio of P and $e_1(\mathbf{r}_1)A_1/n_1 - e_2(\mathbf{r}_2)A_2/n_2$ is almost the same for the four points and this ratio is close to the theoretical value of β.

Thirdly, the spring is successively attached on a point located at the intersection of the lines ($\mathbf{s}_1$, $\mathbf{s}_2$, $\mathbf{s}_3$, and $\mathbf{s}_4$). The exchanged power is increased by a step of $10\log(9/4)$ which corresponds to the enhancement factor of 9/4. The ratio of the exchanged power P and $e_1(\mathbf{r}_1)A_1/n_1 - e_2(\mathbf{r}_2)A_2/n_2$ is almost the same for the four points and this ratio is close to the theoretical value of β.

Whatever the position of the spring attachment, the value of β is found to be in fine agreement with the theoretical value. The mean error is 31.02%.

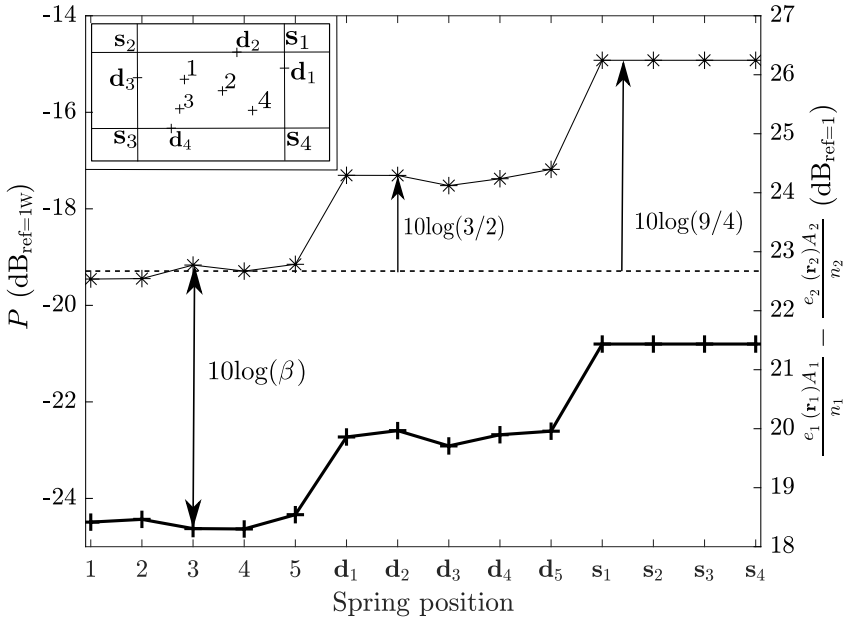

(a)

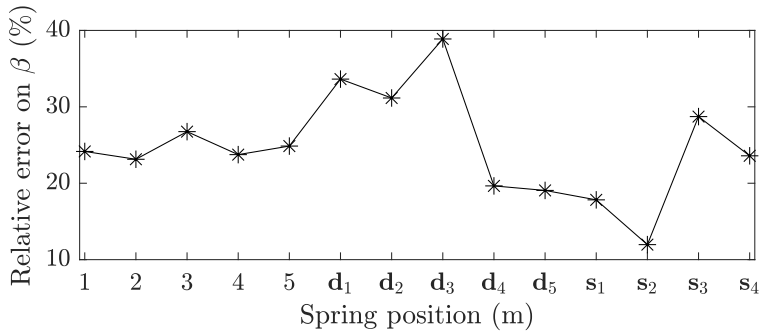

(b)

FIG. 9. (a) Comparison between the exchanged power and the difference of local energies. The bold line with the crosses represents the power exchanged between the two plates. The thin line with the stars represents the difference of the local energies. In the insert: Rectangular plate excited with a random white noise at point $\mathbf{s}_1$. Lines with an energy enhancement equal to 3/2 are represented with lines and the energy enhancement at these lines intersections is 9/4. The spring is successively attached to the points noted $\mathbf{s}_1$, $\mathbf{s}_2$, $\mathbf{s}_3$, $\mathbf{s}_4$, $\mathbf{d}_1$, $\mathbf{d}_2$, $\mathbf{d}_3$, $\mathbf{d}_4$, $\mathbf{d}_5$, 1, 2, 3, 4 and 5. (b) Relative error between the coupling coefficient predicted theoretically with Eq. (3) and numerically with Eq. (10) for two coupled rectangular plates excited by a point force on plate 1.

3. Circular plate

The numerical simulation with two coupled circular plates is presented in Fig. 10(a). The circular plate is shown in the inset Fig. 10(a). The source is located at point $\mathbf{s}_1$. The energy enhancement is represented with the dashed circle noted C_1. Fig. 10(a) shows a comparison between the exchanged power P and the difference of local energies $e_1(\mathbf{r}_1)A_1/n_1 - e_2(\mathbf{r}_2)A_2/n_2$. Fig. 10(b) shows the relative error between β determined by Eq. (3) and by Eq. (10).

The exchanged power P and the difference of local energies $e_1(\mathbf{r}_1)A_1/n_1 - e_2(\mathbf{r}_2)A_2/n_2$ are calculated for 108 points along the radius d_1. It can be seen in Fig. 10(a) that the energy is higher on the circle passing through the excitation point and decreases inside and outside of this circle. The ratio of the exchanged power P and the difference of the local energies $e_1(\mathbf{r}_1)A_1/n_1 - e_2(\mathbf{r}_2)A_2/n_2$ is almost the same for all the points and this ratio is very similar to the theoretical value of β.

The coupling coefficient is found to be in fine agreement with the theoretical value. The mean relative error between the numerical and theoretical value of β is 36.8%.

4. Rectangular plate with high damping

The numerical simulation with two rectangular plates with high damping is presented in Fig. 11(a). The rectangular plate is shown in the inset of Fig. 11(a). Fig. 11(a) shows a comparison between the exchanged power P and the difference of local energies

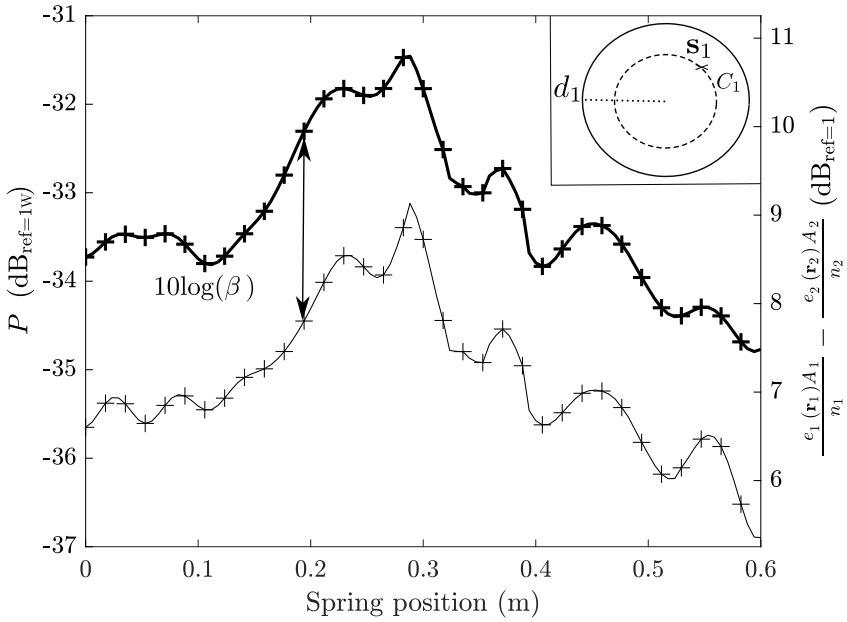

(a)

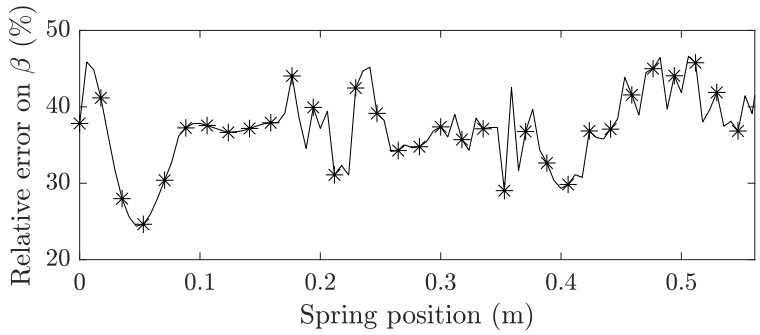

(b)

FIG. 10. (a) Comparison between the exchanged power and the difference of local energies. The bold line with the crosses represents the power exchanged between the two plates. The thin line with the stars represents the difference of the local energies. In the insert: Circular plate excited with a random white noise at point $\mathbf{s}_1$ on the plate 1. The circle with an energy enhancement is noted C_1. The spring is successively attached to 108 points along the line d_1. (b) Relative error between the coupling coefficient predicted theoretically with Eq. (3) and numerically with Eq. (10).

$e_1(\mathbf{r}_1)A_1/n_1 - e_2(\mathbf{r}_2)A_2/n_2$. Fig. 11(b) presents the relative error between β determined by Eqs. (3) and (10).

The spring is successively attached at the 108 points along the line d_1. We see in Fig. 11(a) that the exchanged power evolves proportionally to the difference of the local energies. The difference of local energies and the exchanged power are very high at the vicinity of the source point and decrease rapidly. The ratio of P and $e_1(\mathbf{r}_1)A_1/n_1 - e_2(\mathbf{r}_2)A_2/n_2$ is almost the same for the 108 points. Furthermore we see in Fig. 11(b) that this ratio is close to the theoretical value of β given in Eq. (3). The mean relative error between the numerical and the theoretical value of β is 14.06%. This proves that the coupling coefficient is still valid with non diffuse field caused by high damping.

V. MEASUREMENT OF EXCHANGED POWER

Finally, we present measurements of the power exchanged between two rectangular plates coupled with a spring to verify the generalized coupling power proportionality (Eq. 5).

A. Principle of the experiment

The experimental set-up is shown in Fig. 12. The plates are suspended from a rigid frame with bungee cords attached to the plates by small holes. The two plates are coupled with a spring of stiffness K=431 N.m^{-1} held by magnets. The plates are made of stainless steel. The mechanical characteristics of the plates are exactly the same as in Section III excepted that the boundary conditions are now free.

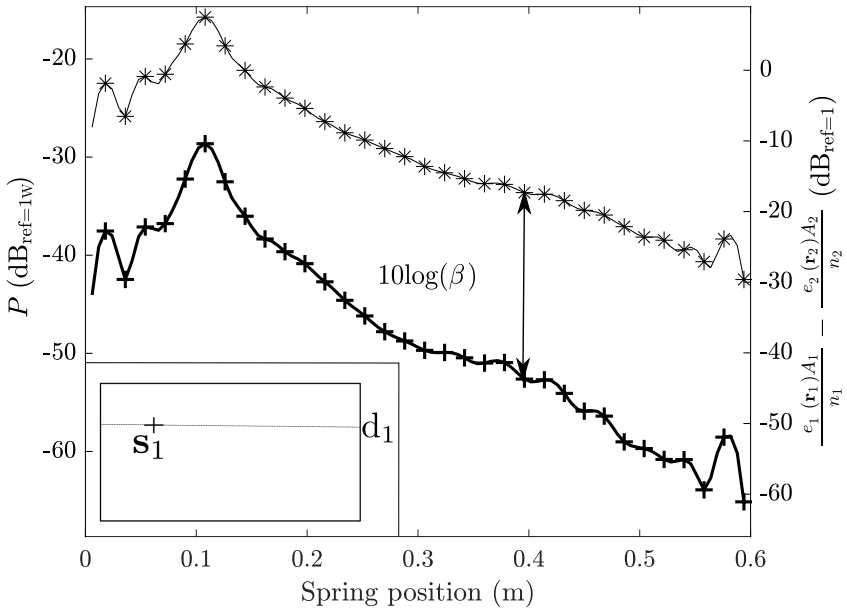

(a)

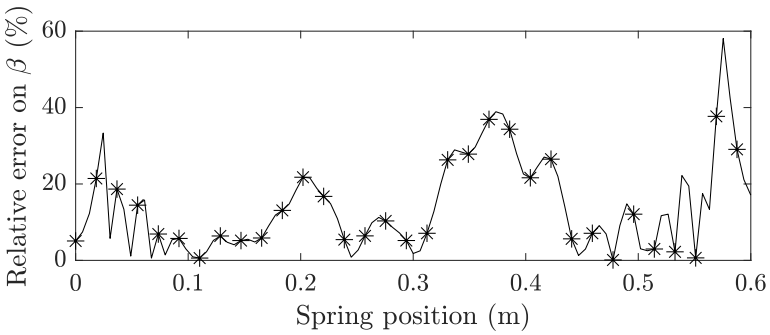

(b)

FIG. 11. (a) Comparison between the exchanged power and the difference of local energies. The bold line with the crosses represents the power exchanged between the two plates. The thin line with the stars represents the difference of the local energies. In the insert: Rectangular plates with high damping excited with a random white noise at point $\mathbf{s}_1$. The spring is successively attached to 108 points along the line d_1. (b) Relative error between the coupling coefficient predicted theoretically with Eq. (3) and numerically with Eq. (10).

The excitation signal is a white noise with a cut-off frequency of 7 MHz generated via a Agilent 33210A signal generator. The signal is then filtered with an SR650 bandpass filter between 10 Hz and 8 kHz and amplified by a Brüel & Kjaer power amplifier type 2718. This filtered signal drives a shaker Brüel & Kjaer type 4810 which applies a transverse force to plate 1.

Two accelerometers PCB 352C67 are attached with wax to the two plates at the position of the spring attachment but on the opposite side. These accelerometers have a sensitivity of 100 mV/g and allow measurements from 0.5 Hz to 10 kHz. The mass of these accelerometers is 2 g which is negligible compared to the mass of the plate which is 2 kg. To measure the force injected into the system, a Brüel & Kjaer impedance head type 8001 is screwed on the shaker. The impedance head is connected to a Brüel & Kjaer type 2635 charge amplifier. The data acquisition is done with a National Instruments NI 9234 acquisition board with a sampling frequency of 12.8 kHz per channel. The averaging is performed with 20 measurements with an overlap factor of 25 % representing an acquisition time of 25.6 s. A Hamming window is applied to each measurement. With the software M+P Analyzer, the time signal is processed and the frequency response function is obtained with the estimator H_2.

To ensure that the energy is transmitted only through the coupling spring and not through the frame, the spring is first disconnected plate 1 being always excited. The energy of plate 2 without the coupling is found 35 dB less than with the coupling. This gives the part of energy transmitted through the frame or the air.

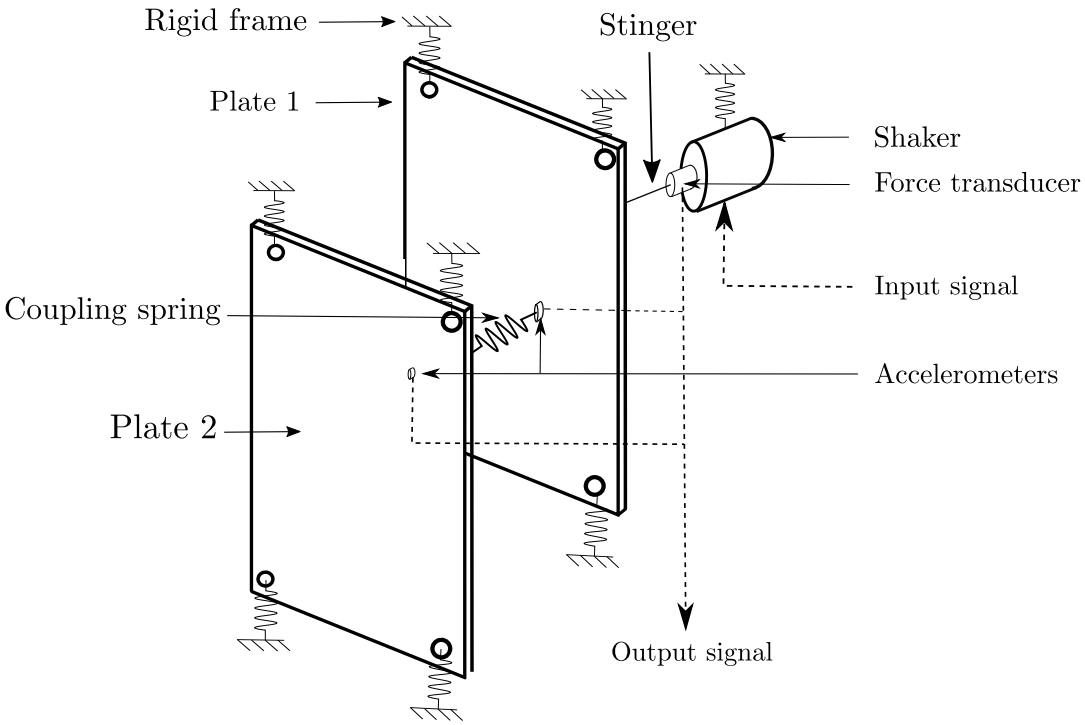

FIG. 12. Experimental set-up. Both plate 1 and 2 are coupled with a spring. The shaker excites plate 1 through the stinger, which is bonded to the plate. The force injected is measured with a force transducer. The acceleration of both plates is measured at the coupling point with the accelerometers.

B. Measurement protocol

The different steps performed to measure the plate energy, the power exchanged and the coupling coefficient are the followings. The excitation is located at point $\mathbf{s}_0$ (x= 0.12 m;

y=0.2 m). The origin of the reference frame is the centre of the plate. The coordinates of the different measurements and coupling points are presented in Table II. $\mathbf{s}_1$ and $\mathbf{s}_2$ are points with an energy enhancement equal to 9/4, $\mathbf{d}_1$, $\mathbf{d}_2$ and $\mathbf{d}_3$ are points with an energy enhancement of 3/2.

TABLE II. Attachment points of spring on plate 1 (m).

$\mathbf{s}_1$	$\mathbf{s}_2$	$\mathbf{d}_1$	$\mathbf{d}_2$	$\mathbf{d}_3$	1	2	3
(0.1; 0,5)	(0.1; 0.1)	(0.1; 0.35)	(0.22; 0.5)	(0.1; 0.25)	(0.25; 0.35)	(0.2; 0.25)	(0.25; 0.2)

For each attachment point of the spring, the measurements are performed five times and the average is calculated. Between each measurement the two accelerometers are taken off and then put back at the same point. A slight variation in measurement is observed due to the thickness of the wax and the slight variation in the measurement position. In order to quantify this uncertainty, 100 measurements are made for measurement point 1 and the standard deviation is calculated and is equal to 0.71 dB.

From accelerometers measurements, the local energy at the coupling points e_1^{exp} and the exchanged power P^{exp} are calculated. Finally the coupling coefficient is calculated with

$$\beta^{exp} = \frac{P^{exp}}{e_1^{exp}(\mathbf{r}_1)A_1/n_1 - e_2^{exp}(\mathbf{r}_2)A_2/n_2}. \tag{11}$$

with A_i the surface of the plate and n_i the modal densities of the plate i determined numerically.

C. Results

The experimental results with two coupled rectangular plates are shown in Fig. 13(a). Fig. 13(a) shows the difference in local energies at the coupling point $e_1^{exp}(\mathbf{r}_1)A_1/n_1 - e_2^{exp}(\mathbf{r}_2)A_2/n_2$ and the exchanged power P^{exp}. Looking at Fig. 13(a), we see that the lines and the points with energy enhancement appear well because the energy on the lines ($\mathbf{d}_i$) and on the points ($\mathbf{s}_i$) is higher than the energy on the rest of the plate. These experimental enhancement factors are very close to the theoretical values. Moreover, the exchanged power evolves in a proportional way to the difference of the local energies.

Fig. 13(b) presents the relative error between the experimental coupling coefficient and the coupling coefficient β given in Eq. (3). The two values agree well and the average error is equal to 25.2%. This validates experimentally for this case the proposed Eq. (5) in cases of inhomogeneous vibrational fields.

VI. THERMODYNAMIC INTERPRETATION

In statistical energy analysis, we use the modal energy E/N where $N = n\Delta\omega$ is the number of resonant modes in the frequency band $\Delta\omega$ and E the total vibrational energy of the subsystem. The subsystem is assumed to be in equilibrium in the sense that the energy E is equally shared between a large number of modes N. In thermodynamics, the temperature is defined for a system at equilibrium (all points of the system have the same energy) as the total energy divided by the number of molecules (or atoms or degrees of

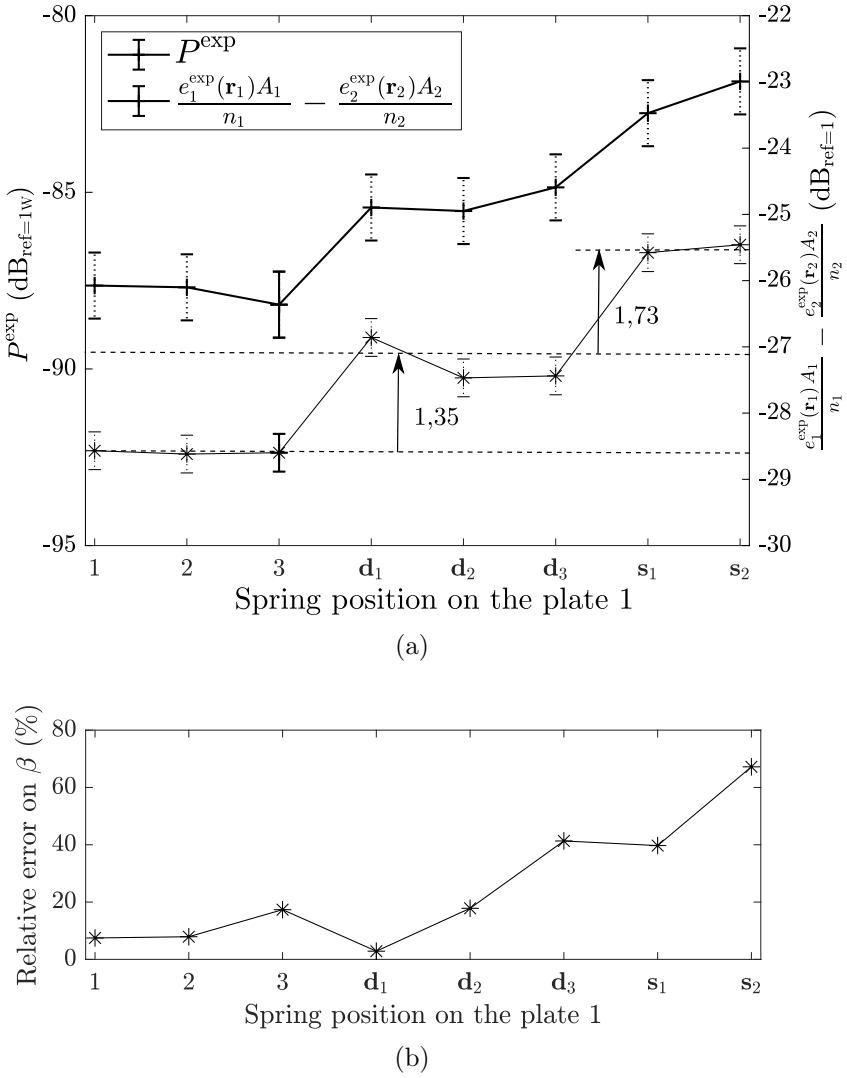

FIG. 13. (a) Comparison between the exchanged powers and the difference of the local energies obtained experimentally. (b) Relative error between the theoretical (β^{th}) and the experimental (β^{exp}) coupling coefficient.

freedom). It is rather common in SEA literature[35] to define the vibrational temperature as

$$T = \frac{E}{k_B N} \tag{12}$$

where k_B is Boltzmann's constant. But, $E = eA$ where e is the energy density and A the system area, and $N = A\omega\Delta\omega/2\pi c_p c_g$ with c_p and c_g the group and phase velocities. The ratio

E/N no longer depends on the area and is therefore a local quantity. It may be interpreted as the local vibrational temperature. When the system is no longer in equilibrium (or when the vibrational field is no longer diffuse), Eq. (5) reads

$$P = \beta k_B \Delta\omega (T_1 - T_2). \tag{13}$$

where now T_1 and T_2 are the local vibrational temperatures at the exchange point. It is now apparent that Eq. (13) states that the power transmitted from subsystem 1 to subsystem 2 is proportional to the difference of local temperatures similarly to the thermal conduction. The coupling power proportionality is similar to Clausius' principle which states that thermal energy always flows from high temperature to low temperature.

VII. CONCLUSION

In this paper, we have highlighted that the requirement of diffuse field in statistical energy analysis may be by-passed provided that the local energies are known at the coupling points. The key result is that a local form of the coupling power proportionality turns out to remain valid even at points where the local energy is not equal to the spatial average of energy.

In order to reach this result, four different systems have been studied with mainly three causes of non-diffuseness. First, spatial symmetries induce energy enhancement by coherence of rays at some particular lines or points (lightly damped rectangular plate or stadium). Second, non-ergodicity may induce a heterogeneity of field due to the presence of caustics (circular plate). Third, high damping frustrates the homogeneity of field by imposing a domination of the direct field (higly damped rectangular plate).

458 Of course, this result does not presume the way by which the information of local energy
459 is obtained. Within the framework of a strict application of statistical energy analysis, this
460 seems to be out of range. However, direct measurements of local energy or application of
461 theoretical enhancement factors can offer insights to improve the predictability of statistical
462 energy analysis. In all other cases, it might also be possible to implement more advanced
463 theories such as ray-tracing or geometrical theory of diffraction for predicting interference
464 effects, dynamical energy analysis or radiative energy transfer to account for non homo-
465 geneity in wave propagation, statistical modal energy distribution analysis for non uniform
466 modal distribution, or even any other theory capable of delivering an information on the
467 distribution of vibrational energy.

468 APPENDIX A: CALCULATION OF RECEPTANCE

469 The calculation of the receptance H of the coupled plates used in equations (6) and (9)
470 is presented in this Appendix.

471 The coupling spring of stiffness K is attached at points $\mathbf{r}_1$ on plate 1 and $\mathbf{r}_2$ on plate 2.
472 A unit harmonic force $\exp(\mathrm{i}\omega t)$ is applied to plate 1 at $\mathbf{s}$ as shown in Fig. 1. We denote by
473 $H(\mathbf{r}, \mathbf{s}; \omega)$ the receptance of the coupled plates with a receiver at $\mathbf{r}$ in plate 1 or 2 and a unit
474 harmonic force at point $\mathbf{s}$ in plate 1. We also denote by $H_i(\mathbf{r}, \mathbf{s}; \omega)$ the receptance of plate i
475 isolated from the other plate.

476 Plate 1 is submitted to two forces: the external force $F = 1$ applied at $\mathbf{s}$ and the force
477 $K(u_2(\mathbf{r}_2) - u_1(\mathbf{r}_1))$ exerted by the spring at $\mathbf{r}_1$. The receptance H at any receiver $\mathbf{r}$ in plate

478 1 is therefore

$$H(\mathbf{r},\mathbf{s};\omega) = H_1(\mathbf{r},\mathbf{s};\omega) + K(u_2(\mathbf{r}_2) - u_1(\mathbf{r}_1))H_1(\mathbf{r},\mathbf{r}_1;\omega); \tag{A1}$$

479 Plate 2 is excited by only one force, the spring reaction at point $\mathbf{r}_2$. The receptance H at
480 any receiver in plate 2 is therefore

$$H(\mathbf{r},\mathbf{s};\omega) = -K(u_2(\mathbf{r}_2) - u_1(\mathbf{r}_1))H_2(\mathbf{r},\mathbf{r}_2;\omega) \tag{A2}$$

481 But the receptance H at $\mathbf{r}_1$ is the deflection $u_1(\mathbf{r}_1)$ and at $\mathbf{r}_2$ the deflection $u_2(\mathbf{r}_2)$.

482 Substituting $\mathbf{r} = \mathbf{r}_1$ in equation (A1) and $\mathbf{r} = \mathbf{r}_2$ in equation (A2) gives

$$\begin{aligned} u_1(\mathbf{r}_1) &= H_1(\mathbf{r}_1,\mathbf{s};\omega) + K(u_2(\mathbf{r}_2) - u_1(\mathbf{r}_1))H_1(\mathbf{r}_1,\mathbf{r}_1;\omega); \\ u_2(\mathbf{r}_2) &= -K(u_2(\mathbf{r}_2) - u_1(\mathbf{r}_1))H_2(\mathbf{r}_2,\mathbf{r}_2;\omega) \end{aligned} \tag{A3}$$

483 This gives a set of two linear equations on the unknowns $u_1(\mathbf{r}_1)$ and $u_2(\mathbf{r}_2)$. Then, the
484 receptance H is obtained with equations (A1) and (A2).

References

[1]R. H. Lyon and G. Maidanik, "Power flow between linearly coupled oscillators," J. Acoust. Soc. Am. **34**(5), 623–639 (1962).

[2]D. Newland, "Calculation of power flow between coupled oscillators," J. Sound Vib. **3**(3), 262–276 (1966).

[3]D. Newland, "Power flow between a class of coupled oscillators," J. Acoust. Soc. Am. **43**(3), 553–559 (1968).

[4]T. D. Scharton and R. H. Lyon, "Power flow and energy sharing in random vibration," J. Acoust. Soc. Am. **43**(6), 1332–1343 (1968).

[5]A. Le Bot, *Foundation of statistical energy analysis in vibroacoustics* (Oxford University Press, 2015).

[6]A. Le Bot, A. Carcaterra, and D. Mazuyer, "Statistical vibroacoustics and entropy concept," Entropy **12**(12), 2418–2435 (2010).

[7]R. L. Weaver, "Diffuse waves in finite plates," J. Sound Vib. **94**(3), 319–335 (1984).

[8]R. H. Lyon, "Needed: a new definition of diffusion," J. Acoust. Soc. Am. **56**(4), 1300–1302 (1974).

[9]L. Maxit and J.-L. Guyader, "Extension of sea model to subsystems with non-uniform modal energy distribution," J. Sound Vib. **265**(2), 337–358 (2003).

[10]G. Zhu, L. Maxit, N. Totaro, and A. Le Bot, "A hybrid modal/statistical formulation for predicting the energy response of vibroacoustic systems in the mid frequency range," J. Sound Vib. **538**, 117221 (2022).

[11]A. Le Bot, "A vibroacoustic model for high frequency analysis," J. Sound Vib. **211**, 537–554 (1998).

[12]A. Le Bot and A. Bocquillet, "Comparison of an integral equation on energy and the ray-tracing technique in room acoustics," J. Acoust. Soc. Am. **108**, 1732–1740 (2000).

[13]A. Le Bot, "Energy transfer for high frequencies in built-up structures," J. Sound Vib. **250**, 247–275 (2002).

[14]A. Le Bot and E. Sadoulet-Reboul, "High frequency vibroacoustics: A radiative transfer equation and radiosity based approach," Wave Motion **51**(4), 598–605 (2014).

[15]G. Tanner, "Dynamical energy analysis-determining wave energy distributions in vibro-acoustical structures in the high frequency regime," J. Sound Vib. **320**, 1023–1038 (2009).

[16]G. Tanner and S. Giani, "Wave transport in complex vibro-acoustic structures in the high-frequency limit," in *Symposium on the vibration analysis of structures with uncertainties*, edited by A. K. Belyaev and R. Langley, Springer (2011), pp. 187–200.

[17]T. Hartmann, S. Morita, G. Tanner, and D. Chappell, "High frequency structure- and air-borne sound transmission for a tractor model using dynamical energy analysis," Wave Motion **87**, 132–150 (2019).

[18]A. Le Bot, "Derivation of statistical energy analysis from radiative exchanges," J. Sound Vib. **300**(3-5), 763–779 (2007).

[19]B. Mace, "Power flow between two continuous one-dimensional subsystems: a wave solution," J. Sound Vib. **154**(2), 289–319 (1992).

[20]G. Maidanik and J. Dickey, "Wave derivation of the energetics of driven coupled one-dimensional dynamic systems," J. Sound Vib. **139**(1), 31–42 (1990).

[21]R. Lyon and E. Eichler, "Random vibration of connected structures," J. Acoust. Soc. Am. **36**, 1344–54 (1964).

[22]W. Wöhle, T. Beckmann, and H. Schreckenbach, "Coupling loss factors for statistical energy analysis of sound transmission at rectangular structural slab joints, part i," J. Sound Vib. **77**(3), 323–334 (1981).

[23]K. Itao and S. Crandall, "Wide-band random vibration of circular plates," Transactions of the ASME **100**, 690–695 (1978).

[24]A. Langley and P. Taylor, "Chladni patterns in random vibration," International Journal of Engineering Science **17**(9), 1039–1047 (1979).

[25]A. Le Bot, O. Robin, K. Rouard, and A. Berry, "Analysis of random mechanical vibrations in symmetrical thin plates using full-field vibration measurements," Journal of Vibration and Acoustics **143**(2), 024503 (2021).

[26]V. Tyrode, N. Totaro, L. Maxit, and A. Le Bot, "Coherent wave reflection in integrable or chaotic symmetrical acoustical billiards," Proceedings of the Royal Society A **477**(2255), 20210488 (2021).

[27]T. Lafont, N. Totaro, and A. Le Bot, "Review of statistical energy analysis hypotheses in vibroacoustics," Proc. R. Soc. A **470**(2162), 20130515 (2014).

[28]T. Lafont, N. Totaro, and A. Le Bot, "Coupling strength assumption in statistical energy analysis," Proc. R. Soc. A **470**(2162), 20130515 (2017).

[29]A. Keane and W. Price, "Statistical energy analysis of strongly coupled systems," J. Sound Vib. **117**(2), 363–386 (1987).

[30]F. Fahy and Y. de Yuan, "Power flow between non-conservatively coupled oscillators," J. Sound Vib. **114**, 1–11 (1987).

[31]A. Le Bot and V. Cotoni, "Validity diagrams of statistical energy analysis," J. Sound Vib. **329**(2), 221–235 (2010).

[32]A. Le Bot, Z. Bazari, P. Klein, and J. Lelong, "Statistical analysis of vibration in tyres," J. Sound Vib. **392**, 187–199 (2017).

[33]H. Li, N. Totaro, L. Maxit, and A. Le Bot, "Ergodic billiard and statistical energy analysis," Wave Motion **87**, 166–178 (2019).

[34]G. Tanner and N. Søndergaard, "Wave chaos in acoustics and elasticity," J. Phys. A: Math. Theor. **40**(50), R443–R509 (2007).

[35]A. Le Bot, "Entropy in statistical energy analysis," J. Acoust. Soc. Am. **125**(3), 1473–1478 (2009).